

The Mutual Interaction between Continental-Scale Ice Sheets and Atmospheric Stationary Waves

GERARD H. ROE

Quaternary Research Center, University of Washington, Seattle, Washington

RICHARD S. LINDZEN

Program in Atmospheres, Oceans, and Climate, Massachusetts Institute of Technology, Cambridge, Massachusetts

(Manuscript received 10 December 1999, in final form 12 June 2000)

ABSTRACT

The great continental ice sheets of the Pleistocene represented significant obstacles to the Northern Hemisphere midlatitude westerlies. They must therefore have forced large changes in the atmospheric circulation, and consequently also in the patterns of accumulation and melting over the ice sheets themselves. A simplified three-dimensional coupled ice sheet–stationary wave model is developed in order to understand the ice sheet’s response to the circulation changes that it induces. Consistent with ice age climate simulations, the ice sheet topography induces an anticyclonic circulation over the ice sheet, causing a slight warming over the western slopes and a stronger cooling over the remainder. The modeled feedbacks significantly affect the ice sheet configuration, with the most important influences being the patterns of summer temperature, and the topographically induced precipitation field. The time evolution of the ice sheet is also changed by the atmospheric feedbacks and the results suggest the possibility of multiple equilibrium solutions.

1. Introduction

At the last glacial maximum (LGM) at 21 kbp (thousands of years before present), the Laurentide ice sheet extended over much of what is now Canada and reached a height of over 3 km. The Fennoscandian ice sheet was slightly smaller in extent and height. These two enormous ice masses, which were comparable in size to the Tibetan Plateau, sat year-round in the midlatitude westerlies and must have been substantial sources of atmospheric stationary waves. When the midlatitude westerlies are forced around such large-scale topography, significant deviations from the zonal mean climate arise. Moreover the downstream propagation of the waves influences the climate far from the source region. Figure 1 shows that in today’s winter climate, for example, there is a roughly 10°C east–west temperature difference in the lower troposphere across each of the two major mountain complexes, the Rockies and the Tibetan Plateau. To be sure, other zonal asymmetries in climate forcing such as latent heating and the land–sea thermal contrast also contribute to this pattern.

The propagation of stationary wave patterns away from the source region is very sensitive to the details of the atmospheric structure and even a small change in the phase of the pattern makes a big difference to the local climate (e.g., Nigam and Lindzen 1989). Significant climate changes can therefore be caused by even small adjustments in stationary wave patterns. By way of comparison, high-latitude temperature differences between glacial and interglacial climates are thought to have been about 10°C (e.g., Crowley and North 1991) and so the reorganization of the atmospheric circulation by the great ice sheets was likely a zeroth-order local climate forcing during peak glaciations.

An ice sheet is a dynamical entity. The accumulation of snow in the interior is gradually compressed into ice by succeeding years’ accumulation and is slowly incorporated into the main body of ice. The increasing load builds up stresses within the ice, which responds by gradually redistributing its mass over thousands of years. The outward flow of ice is balanced by calving (shedding of icebergs) at a coast, and summer ablation (melting) at a land-based margin (e.g., Tangborn and Simont 1988).

The accumulation and melting patterns are in turn a function of the winds and temperatures over the ice sheet. Given this direct link between atmospheric circulation and ice sheet mass balance, the main purpose

Corresponding author address: Dr. Gerard H. Roe, Quaternary Research Center, University of Washington, Box 351360, Seattle, WA 98195-1360.
E-mail: groe@alum.mit.edu

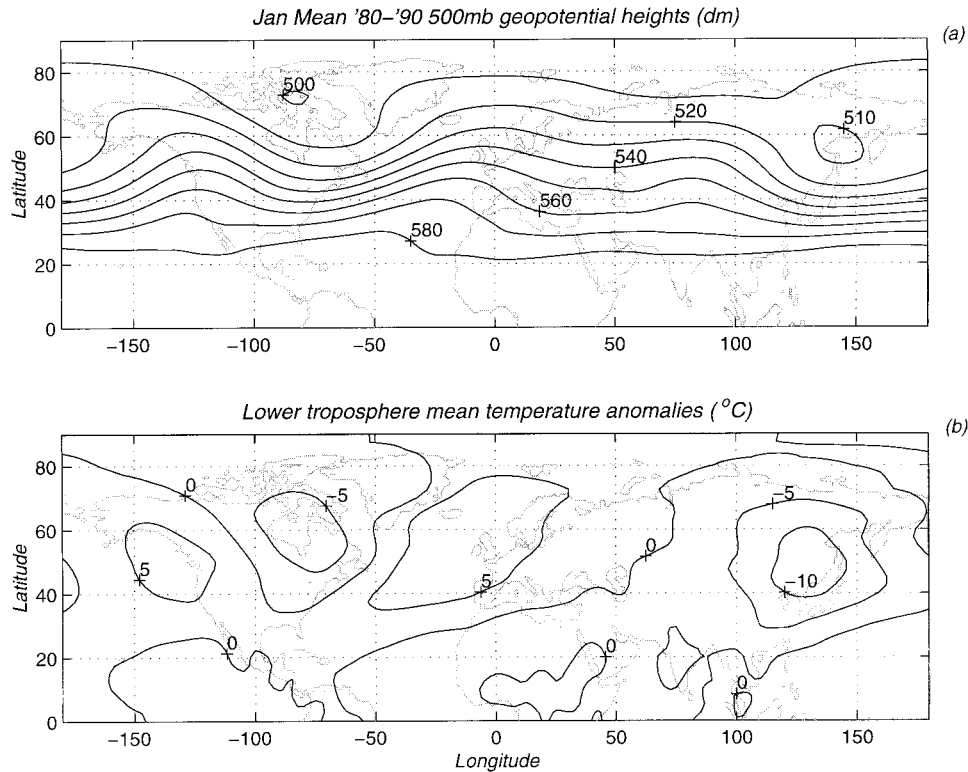


FIG. 1. Observed Jan stationary wave. The National Centers for Environmental Prediction reanalysis data (Kalnay et al. 1996), average from 1980 to 1990. (a) The 500-mb geopotential heights (dam), and (b) perturbation of lower-tropospheric temperature from the zonal mean ($^{\circ}\text{C}$), calculated by equating the 1000–500-mb thickness to a vertical mean temperature.

of this paper is to understand how the presence of a continental-scale ice sheet influences the surrounding climate and how the altered patterns of accumulation and ablation feed back onto the shape and size of the ice sheet. The question is obviously important in understanding the evolution of the ice ages. However, previous studies have tended to be either general circulation model (GCM) “snapshot” simulations with imposed and fixed boundary conditions, unable to account for the response of the ice dynamics (e.g., Kutzbach and Guetter 1986; Hall et al. 1996), or energy balance model (EBM) simulations in which long-timescale integrations are possible, but there is no modeling of the atmospheric dynamics, except as providing a diffusive heat flux (e.g., Tarasov and Peltier 1997).

Roe and Lindzen (2001) used a one-dimensional model to show that if circulation changes induces a temperature perturbation at an ice sheet’s southern margin proportional to its height, then its time evolution and equilibrium shape of the ice sheet are significantly affected. The present paper extends the earlier study to three dimensions while maintaining the simplest framework necessary to model the interaction. A linear quasigeostrophic model is used to represent the atmosphere, partly motivated by the results of Cook and Held (1988) who showed that, at least in winter, the stationary wave

pattern over North America in a GCM simulation at the LGM was mostly a linear response to the topographic forcing. A parameterization for the precipitation distribution is presented that emphasizes the role of topography. Using simplified geometry, model integrations presented in section 3 show that when an ice sheet is allowed to evolve to equilibrium in concert with the circulation changes it induces, both the temperature patterns in the atmospheric flow and the topographic effects on precipitation cause large changes in the ice sheet’s configuration and dynamics. In addition multiple equilibrium solutions are possible if different initial ice sheet shapes are used. Section 4 shows that the growth of an ice sheet is strongly affected by the examined feedbacks, particularly if the ice sheet initiates away from the west coast of the continent. There is a summary and discussion of the results in section 5.

2. Model description

a. Stationary wave model

The atmospheric component of the model is a linear, quasigeostrophic, stationary wave model in a beta plane channel. The equations used are similar to Lindzen (1994) or Pedlosky (1992), so will just be outlined here.

The atmospheric fields are linearized about a basic state that is a function of height only. That is, $u(x, y, z) = \overline{U}(z) + u'(x, y, z)$, $T = \overline{T}(z) + T'(x, y, z)$, where u is the zonal wind, T is the temperature, an overbar denotes the basic state, and a prime denotes a perturbation field. Here z is a scaled log pressure coordinate:

$$z = -H \ln(p/p_0), \quad (1)$$

where H is the fixed scale height (set at 7.5 km), and p_0 is a reference pressure. Combining the vorticity and thermodynamic equations gives the linearized conservation of quasigeostrophic potential vorticity (PV) equation for the interior of the domain (e.g., Lindzen 1994):

$$\overline{U} \frac{\partial q'}{\partial x} + v' \overline{q}_y + \frac{1}{\tau} \frac{\nabla_h^2 \phi'}{f_0} + f_0 e^{z/H} \frac{\partial}{\partial z} \left(\frac{e^{-z/H}}{N^2} \frac{1}{\tau} \frac{\partial \phi'}{\partial z} \right) = 0, \quad (2)$$

where v' is the perturbation meridional wind, ϕ is the geopotential height, N^2 is the square of the Brunt–Väisälä frequency, f_0 is the Coriolis parameter and ∇_h is the horizontal nabla operator. Linear damping with a time-scale of $\tau(z)$ has been applied to the momentum and the temperature equations, and is specified as a function of height. Here, q' is the perturbation PV,

$$q' = \frac{1}{f_0} \nabla_h^2 \phi' + f_0 e^{z/H} \frac{\partial}{\partial z} \left(\frac{e^{-z/H}}{N^2} \frac{\partial \phi'}{\partial z} \right), \quad (3)$$

and \overline{q}_y is the basic-state (background) meridional PV gradient:

$$\overline{q}_y = \beta - e^{-z/H} \frac{d}{dz} \left(\frac{f_0^2}{N^2} e^{-z/H} \frac{d\overline{U}}{dz} \right). \quad (4)$$

The lower boundary condition comes from the thermodynamic equation, together with the constraint that the vertical velocity be zero at the surface. After some manipulation, and again following Lindzen (1994), this can be expressed as

$$\overline{U} \frac{\partial}{\partial x} \left(\frac{\partial \phi'}{\partial z} \right) - \frac{\partial \phi'}{\partial x} \left(\frac{\partial \overline{U}}{\partial z} \right) + \frac{1}{\tau} \frac{\partial \phi'}{\partial x} = -N^2 \overline{U} \frac{\partial z_s}{\partial x}. \quad (5)$$

Here $z_s(x, y)$ is the surface height, and so the term on the right-hand side (rhs) of Eq. (5) represents the forced ascent of the air over the topography. There is some ambiguity about the appropriate forcing wind to use on the rhs of Eq. (5). The boundary condition should strictly be applied at the surface, but the linearization has implicitly assumed that the topography does not stick out into the fluid domain. However in reality the wind impinging of the side of the topography will be larger than the surface wind, and we use the 1-km wind instead (denoted \overline{U}_f). The model's upper boundary has a radiation condition (e.g., Pedlosky 1992). The northern wall of the channel is placed at 90°N and the southern wall is placed sufficiently far south that, with the applied damping, the return reflection of waves are unimportant.

We calculate f_0 and β at 60°N because we are interested in the response at high midlatitudes.

Since Eqs. (2) and (5) are linear, they can be solved for each spectral component of the topography using standard algorithms, and the individual solutions summed to give the total response.

b. Atmospheric basic state

The atmospheric structure appropriate for a glacial climate is not known and therefore we have to choose one that seems reasonable. As demonstrated below, it is the summer temperatures that are crucial for an ice sheet's evolution and so the basic state should be taken to reflect a glacial summer. We will in any event show results for weaker and stronger stationary wave responses in section 3e. The standard basic state used in the model integrations is shown in Fig. 2. The jet strength (23 m s⁻¹ at 10 km) is stronger than for the current climate at 60°N, and reflects the expected increase in baroclinicity during a glacial climate (e.g., Crowley and North 1991). Via the thermal wind balance, the vertical wind shear implies a meridional temperature gradient of -6.6°C/1000 km. The forcing velocity, \overline{U}_f , is 5 m s⁻¹, the tropospheric lapse rate is -6.5°C km⁻¹, and the 0°C isotherm is taken to lie at 50°N. The damping time, τ , is 5 days near the surface, transitioning smoothly to 30 days in the free troposphere. The details of the atmospheric basic state above 10 km do not affect the response close to the surface (Lindzen and Roe 1997).

c. Ice sheet model

The model geometry is simplified in order to focus on the interaction between the ice sheet and the atmosphere. The ice sheet is allowed to exist on a single rectangular continent, roughly the size of North America, with boundaries at 40°N, 70°N, 130°W, and 50°W. Any ice flux across these boundaries is assumed to calve into the ocean, and the height at the margin is set to zero. When there is no ice loading, the continent is assumed to be flat. The model setup is schematically illustrated in Fig. 3.

The ice sheet model used is a simplified version of the SICOPOLIS model (Greve 1997). In it, ice is treated as an isotropic, incompressible, nonlinear, viscous, heat-conducting fluid, with the equations scaled using the shallow ice approximation (e.g., Hutter 1983). It obeys Glenn's flow law; the strain rate responds as the third power of the applied stresses (e.g., Paterson 1994). We further neglect the temperature dependence of the flow, setting the internal ice temperature at a constant -10°C. The ice is assumed to have a stress-free upper surface, and a no-slip lower boundary condition. The model assumes that the bedrock and ice sheet relax toward isostatic equilibrium with a timescale of 3 kyr (thousands of years).

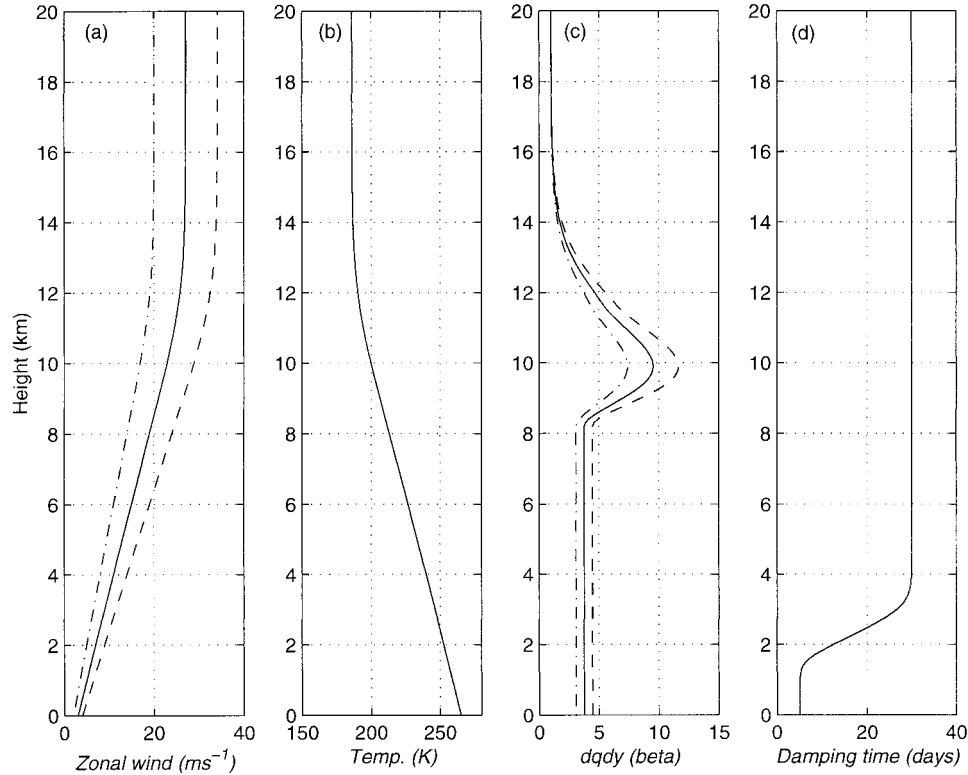


FIG. 2. Atmospheric basic states used in stationary wave model. (a) Zonal winds (m s^{-1}), (b) temperature (K), (c) PV gradients in units of beta ($=1.13 \times 10^{-11} \text{ m}^{-1} \text{ s}^{-1}$), and (d) damping time (days). The solid line gives the standard basic state used in integrations section 3, and where plotted the dashed line is the state used for the strong stationary wave sensitivity and the dash-dotted was that for the weak sensitivity in section 3e. Basic-state details above the tropopause do not affect the surface response.

d. Accumulation parameterization

The ice sheet and the atmospheric components of the model interact with each other via accumulation and ablation at the ice sheet surface. Of necessity we must use very simplified representations, but we can hope to include the relevant physics. For the precipitation we focus particularly on topographic effects. If prevailing winds are upslope, then the air column cools, saturates, and enhanced precipitation results. If on the other hand the winds are downslope, then the adiabatic warming of the air column reduces the precipitation, causing the well-known rain shadow that is observed in the lee of major mountain ranges in today's climate (e.g., Smith 1979). For an ice sheet the topographic influence on precipitation is especially significant because the snowfall is eventually incorporated into the ice sheet and thus influences its shape over time.

The parameterization used here is related to that of Sanberg and Oerlemans (1983) who first demonstrated the importance of topographically influenced precipitation on an ice sheet. We take the precipitation as being proportional to the saturated vapor pressure, e_{sat} , which is an exponential function of the surface temperature, T_s (e.g., Holton 1992). Precipitation therefore decreases with height and latitude. The topography is accounted

for by including a term proportional to the vertical velocity, w . We allow some variability in w , representing transient weather systems or frontal passages. This ensures that even if the prevailing winds are strongly downslope, the parameterization allows for some fraction of time where the vertical velocity is positive, and some snow falls. For the fraction of time for which w is between w' and $w' + dw'$, the precipitation is taken to be

Precipitation rate

$$= e_{\text{sat}}(T_s) \times \max[0, (a + bw')]f(w') dw'. \quad (6)$$

Here $f(w')$ is the probability of w being between w' and $w' + dw'$, and is defined below. The coefficient a gives the background precipitation rate in the absence of topography, and is taken to be $2.5 \times 10^{-11} \text{ m}^2 \text{ s kg}^{-1}$. The value of b may either be derived by comparing Eq. (6) to a steady-state water budget (Roe 1999), or by taking a value derived from observations (Sanberg and Oerlemans 1983; see also Roe 1999). Both approaches result in very similar numbers, and this lends confidence that the parameterization produces physically reasonable precipitation rates. We take b to be $5.9 \times 10^{-9} \text{ m s}^2 \text{ kg}^{-1}$. For $f(w')$ we take a Gaussian distribution cen-

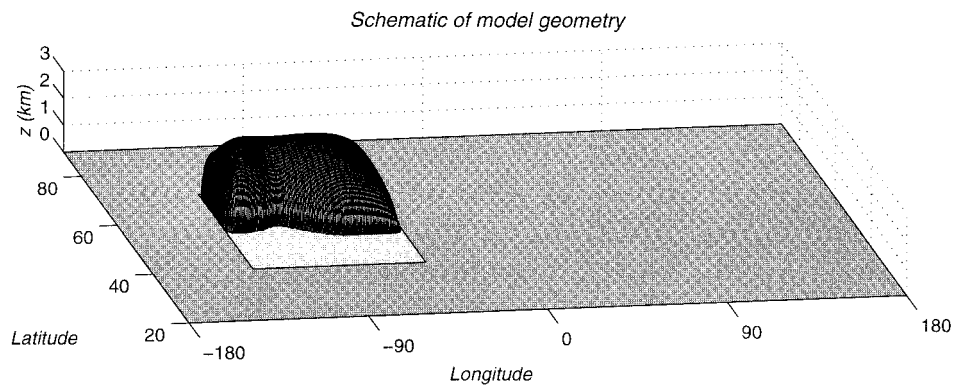


FIG. 3. Schematic of model geometry. The ice sheet is allowed to evolve on the rectangular continent within the channel domain of the atmospheric stationary wave model. The southern boundary of the channel is at a distance equivalent to a lat of 90°S . With the applied damping, this was sufficient to prevent return reflections influencing the solution over the ice sheet. A radiation condition is applied at $z = 20$ km.

tered on the topographically forced vertical velocity, $w = \mathbf{u}(x, y) \cdot \nabla_{h,z_s}(x, y)$.

$$f(w')dw' = \frac{e^{-\alpha^2(w'-w)^2}}{N}. \quad (7)$$

We take $1/\alpha$ as 1 cm s^{-1} , consistent with variations of vertical velocity on synoptic scales. The normalization factor N ensures that $\int_{-\infty}^{\infty} f(w') dw' = 1$. The precipitation rate for a given surface temperature is found by integrating Eq. (6) over the range of w' that gives a positive precipitation rate. In the appendix it is shown how the integral can be reduced to an expression involving error functions, for which there are very accurate asymptotic expansions available. Because the perturbation velocities are included in calculating w , the parameterization takes account of the prevailing wind direction in determining where the upslope or downslope flow occurs.

The annual accumulation is found by integrating the

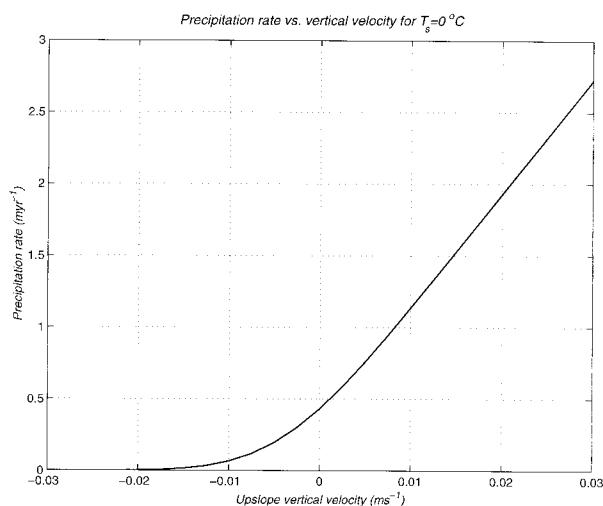


FIG. 4. Precipitation rate as a function of vertical velocity. The curve is what is given by Eq. (6) for $T_s = 0^{\circ}\text{C}$.

precipitation rate of the annual cycle in surface temperature, T_s . It is assumed to fall as snow when T_s is below freezing. If the vertical velocity is set to zero, then for an annual temperature variation of $T_s = 10^{\circ}\text{C} \sin(2\pi t)$, Eq. (6) gives the annual precipitation as 54 cm, of which 16 cm (water equivalent) falls as snow. The dependence of the precipitation rate on w is shown in Fig. 4.

Equation (6) has neglected moisture convergence in the air column due to the stationary wave dynamics. By comparing Eq. (6) to a steady-state moisture budget, it is possible to show that while the wave dynamics are not completely negligible, the forced topographic vertical motion is generally the larger contribution to column moisture convergence over the ice sheet (Roe 1999).

e. Ablation parameterization

We use the positive degree day (PDD) approach to parameterize ablation (Braithwaite and Oleson 1989; Reeh 1991). The amount of PDDs in a year is equal to the integral of the positive temperatures over that year. These accumulated positive temperatures can be regarded as a melting potential. Initially the year's accumulation is melted at a rate β_1 per PDD. Up to 60% of the years accumulation is assumed to percolate down into the snowpack and refreeze, after which point the firn is assumed to become saturated. If there are still remaining PDDs they are then used to melt the superimposed ice (i.e., the refrozen snowmelt) as well as the underlying ice at a rate β_2 per PDD. The meltwater thereby produced is assumed to run off the ice sheet. The different values of β reflect the different albedos of snow and ice. We take $\beta_1 = 1.2 \text{ m }^{\circ}\text{C}^{-1} \text{ yr}^{-1}$ and $\beta_2 = 2.8 \text{ m }^{\circ}\text{C}^{-1} \text{ yr}^{-1}$ (Calov and Hutter 1996).

In reality, snow- and icemelt is the result of many complex processes. A complete treatment would have to involve shortwave and longwave radiation, air and surface temperature, cloudiness, surface albedo, atmo-

spheric humidity, surface wind speeds and shear, and obviously cannot be attempted in such a simple model. However, the choice of melting parameterization is not crucial in this process study: the important property required is that, as observed over ice sheets, the melting be concentrated at the ice sheet margin and during the summer.

3. Equilibrium model integrations

In the previous section the necessary model components were developed to study the interaction between an evolving ice sheet and the responding atmospheric circulation. We now present the results of integrating the coupled model to equilibrium. In order to clearly show the effects of the different process, we isolate in turn the stationary wave and topographic-precipitation feedbacks, and then show their combined effect on the ice sheet's configuration. The model integrations begin with an ice-free continent, and flat bedrock topography. The basic-state climate parameters, defined in the previous section, are such that the ice sheet begins to grow. Every 50 years of model integration, the ice sheet topography is spectrally decomposed and the stationary wave response is calculated. From the diagnosed winds and temperatures, the accumulation and ablation rates are integrated over the annual cycle [i.e., Eq. (8)]. These fields are then interpolated onto the ice sheet model grid (which has a 40 km) resolution, and applied to the ice sheet model for the succeeding 50 years of model integration.

The annual surface temperature variation across the model domain, $T_s(x, y, z_s, t)$, has several components to it:

$$\begin{aligned}
 T_s[x, y, z_s(x, y), t] &= \underbrace{\bar{T}_y(y - y_{fz})}_I + \underbrace{\Gamma z_s(x, y)}_{II} + \underbrace{T_a \sin(2\pi t)}_{III} \\
 &+ \underbrace{T'(x, y)}_{IV}
 \end{aligned} \quad (8)$$

Here \bar{T}_y is the meridional temperature gradient, Γ is the atmospheric lapse rate, and y_{fz} is the latitude of the annual mean 0°C isotherm. Terms I and II give that the temperature decreases with increasing surface height and latitude. Term III is the seasonal cycle for which we choose $T_a = 10^\circ\text{C}$, and term IV is the temperature perturbation given by the stationary wave response.

The seasonal variation of the atmospheric structure (and thus of the stationary wave response) has been neglected here. At high midlatitudes in today's climate, the variation is actually quite small; while the jet is stronger in winter, its maximum is farther north in summer, and the two effects tend to cancel out for some purposes: at 60°N the tropopause jet strength is between 15 and 20 m s⁻¹ year round (e.g., Peixoto and Oort

1992). Experiments including a four-stage annual cycle (i.e., each season with a different basic state) showed that because almost all melting occurs in summer, the ablation patterns were dominated by the summer stationary wave response. Nor were the patterns of annual accumulation changed very much by adding the seasonally varying basic state (Roe 1999). Therefore the simpler approach was taken and T' in Eq. (8) should be interpreted as the summer response.

In the results presented below, most of the stationary wave fields will be shown at $z = 1$ km. A consequence of the linearity assumption is that the perturbation fields exist at all levels even within the topography. In reality the fields change quite slowly with height, and so this unphysical situation is not serious for the calculation.

a. No feedbacks

In equilibrium an ice sheet is a dynamic balance between the integrated accumulation over its interior and melting and/or calving at the margin. This is illustrated in Fig. 5, which shows an integration in which the two feedbacks are not included. The temperature is fixed as zonally symmetric (but still decreasing northward), and b in Eq. (6) is set to zero (i.e., the precipitation is a function of height and latitude only). This must result in a symmetric ice sheet.

In Fig. 5 the divergence of flux from the interior of the ice sheet is about 3 m yr⁻¹ at the southern margin. This is almost exactly balanced by melting during the summer, when the temperature reaches about 5°C. The accumulation at the margin is only about 0.2 m yr⁻¹ and thus a small fraction of the mass budget there. This is why simulations of LGM ice sheets have been found to be quite insensitive to the details of accumulation at the margin (Tarasov and Peltier 1997).

Ice flow is diffusive, so small-scale details in the precipitation distribution do not affect the overall configuration of the ice sheet. The position of the margin is also quite insensitive to changes in integrated interior accumulation rate, because of the strong functional dependence of the ablation on temperature (Fig. 5d). If the accumulation rate were doubled, then, all else being equal, the southward ice flux at the margin would double. However, Fig. 5d shows that the margin would have to advance only a few degrees southward in order to find summer temperatures warm enough to balance the increased ice flux.

b. Precipitation feedback

In order to isolate the effects of the precipitation feedback, an integration is performed in which the perturbations due to the stationary wave were set to zero. The flow is therefore purely westerly. The precipitation feedback is included and therefore snowfall is enhanced on the westward slopes and reduced on the eastward. Figure 6a shows the resulting equilibrium ice sheet. Precipi-

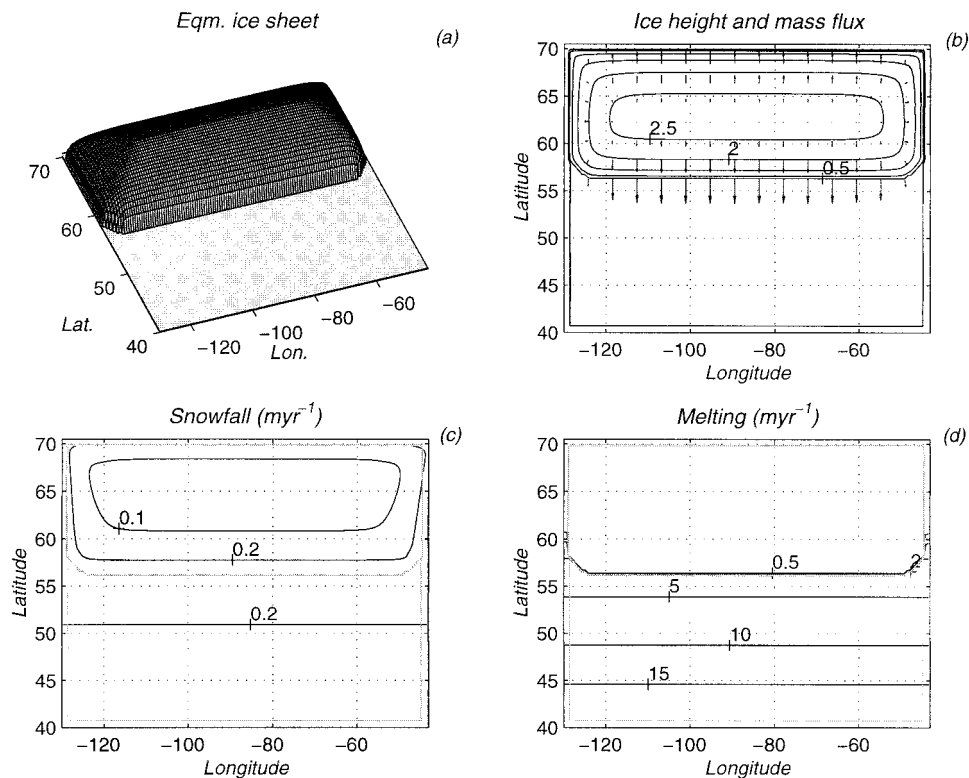


FIG. 5. Model integration with no feedbacks included. The wind and temperature climate forcing is zonally symmetric, and the accumulation is a function only of surface temperature (i.e., adjusted for ice height). (a) The 3D view of ice sheet; (b) ice sheet height contours (every 0.5 km), and vectors of vertically integrated ice mass flux. The largest vector plotted corresponds to $1.0 \times 10^5 \text{ m}^2 \text{ yr}^{-1}$. The largest flux of ice (not plotted because of resolution) is $1.1 \times 10^5 \text{ m}^2 \text{ yr}^{-1}$, giving a maximum ice divergence at the margin of 2.7 m yr^{-1} ; (c) snowfall (m yr^{-1}); (d) melting potential (m yr^{-1}). In (c) and (d) the ice sheet margin is faintly outlined.

tation on the western flank exceeds 3 m yr^{-1} . This snowfall forms ice that quickly flows westward to the coast, where it calves into the ocean. The ice divergence in this region reaches 11 m yr^{-1} , which is balanced by calving into the ocean. However, apart from forcing a small lobe on the southwestern corner of the ice sheet this additional accumulation does not contribute much to the overall shape. On the eastern side of the ice sheet though, the downslope winds cause a large region of precipitation that is 5 cm yr^{-1} or less. This leads to a much weaker ice flux at the margin, which can therefore be balanced by weak summer melting, and the temperature there rises only slightly above 0°C in summer, compared to over 5°C on the western flank. This is reflected in the northward curve of the southern margin.

c. Stationary wave feedback

The effects of the stationary wave circulation alone can be seen by switching off the precipitation feedback [b in Eq. (6) set to zero], and calculating the stationary wave field forced by the ice sheet topography. Figure 7 shows the ice sheet shape is dramatically changed. Compared with the no-feedbacks integration (Fig. 5),

the western margin retreats about 5 degrees north, while the central and eastern portions extend up to 10 degrees south. The height and volume are also increased significantly over the no-feedback integration. The ice sheet topography forces a high pressure anticyclonic circulation centered over the western portion of the ice sheet (Fig. 8c), with an equivalent mean sea level pressure of 1030 mb. This circulation brings up warm southerly air on the western flank (as far east as 105°W). Over most of the ice sheet however, northerly flow of air lowers the temperature to well below the zonal mean climate. There is an east–west temperature difference over the continent of about 10°C (Fig. 7d). Using the meridional temperature gradient this translates to a north–south distance of around 1500 km, which almost entirely accounts for the variation of the ice margin across the continent. The ice margin is largely determined by the summer isotherm pattern and lies roughly on the 5°C isotherm.

While the exact center of the induced high pressure circulation over the topography is dependent on the details of the atmospheric basic state, it is always slightly to the west of the peak of the topography (e.g., Hoskins and Karoly 1981) and therefore northerly prevailing

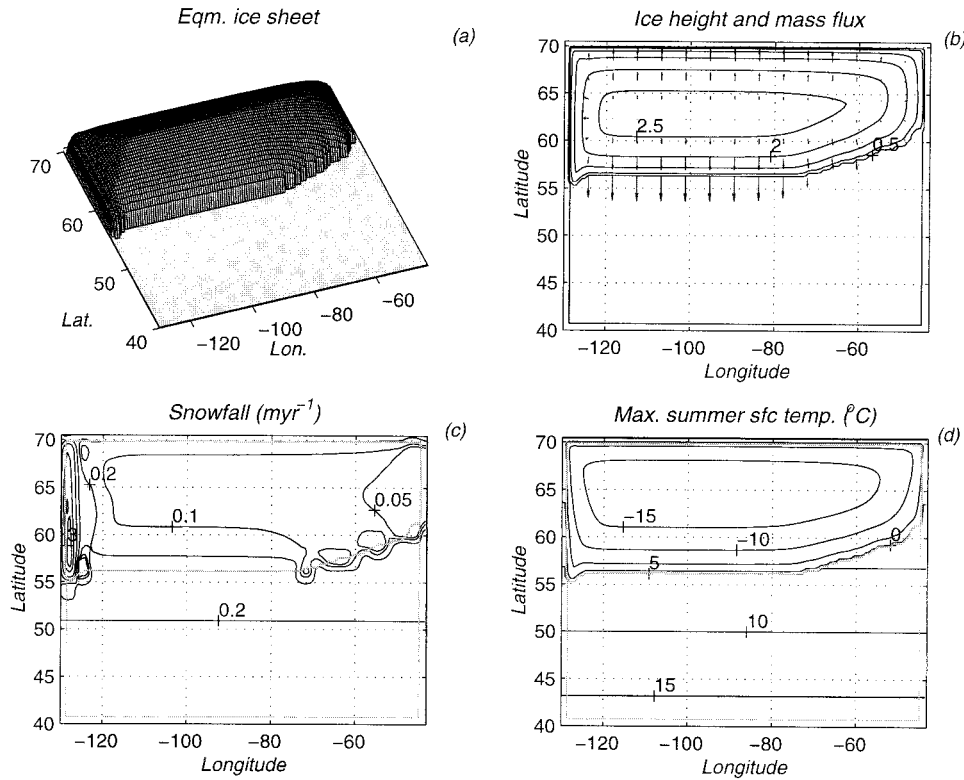


FIG. 6. Model integration with precipitation feedback included. The model wind is fixed as purely zonal, and precipitation is enhanced (suppressed) on the windward (leeward) slopes. Same as Fig. 5, except (b) the largest vector plotted corresponds to $1.0 \times 10^5 \text{ m}^2 \text{ yr}^{-1}$. The largest flux of ice (not plotted because of resolution) is $4.5 \times 10^5 \text{ m}^2 \text{ yr}^{-1}$, giving a maximum ice divergence at the margin of 11.3 m yr^{-1} ; (c) contour intervals used (0.05, 0.1, 0.2, 0.5, 1, 2, 3, 4) m yr^{-1} ; (d) maximum summer temperature ($^{\circ}\text{C}$).

winds will always predominate over most of the ice sheet.

This integration shows the ice sheet margin is strongly influenced by the changes the ice sheet induces in the atmospheric circulation. In the west the margin is forced to retreat because of the induced warm temperatures. Over the rest of the ice sheet the margin is sustained much farther south than it would otherwise be by the cold temperatures associated with the prevailing northerlies. This supports the results of a simpler one-dimensional model Roe and Lindzen (2001), and shows that the diffusive tendency of ice flow (i.e., an east-west spreading) is not sufficient to overcome the temperature patterns in the climate forcing.

d. Combined feedbacks

The equilibrium ice sheet that evolves when both feedbacks are included is shown in Fig. 8. An anticyclonic circulation (not shown) is induced in the atmosphere similar to that in Fig. 7. While the circulation is centered over approximately the same location, the patterns have weaker amplitude because the ice sheet is smaller.

The ice has a slight double-domed structure, reflective

of distinct and different processes at work in the western and eastern sectors. The anticyclonic circulation forces upslope flow (and therefore creates precipitation maxima) on the western and southwestern slopes of the ice sheet. These large accumulation rates (which maximize at about 4 m yr^{-1}) drive a large ice flux within the ice sheet. Since in equilibrium this must be balanced by large melting rates at the land margin, the ice sheet is able to push south to where the summer temperature reaches 8°C before there is sufficient ablation to balance the ice flux. The localized precipitation maxima do not contribute much to the shape of the ice sheet. Rather it is the generally increased precipitation over the whole area that creates the western dome: in an integration in which the precipitation was artificially capped at a maximum of 1 m yr^{-1} , the resulting ice sheet was almost identical to Fig. 8.

Over the remainder of the ice sheet, the prevailing northerlies are generally downslope, creating low-precipitation rates. This produces a mass flux that is an order of magnitude weaker than in the western sector. Very little melting is required to balance this weak flux, and so the summer temperatures just barely make it above 0°C . The southward extension of the ice sheet here is less than for Fig. 7 because of both the reduced

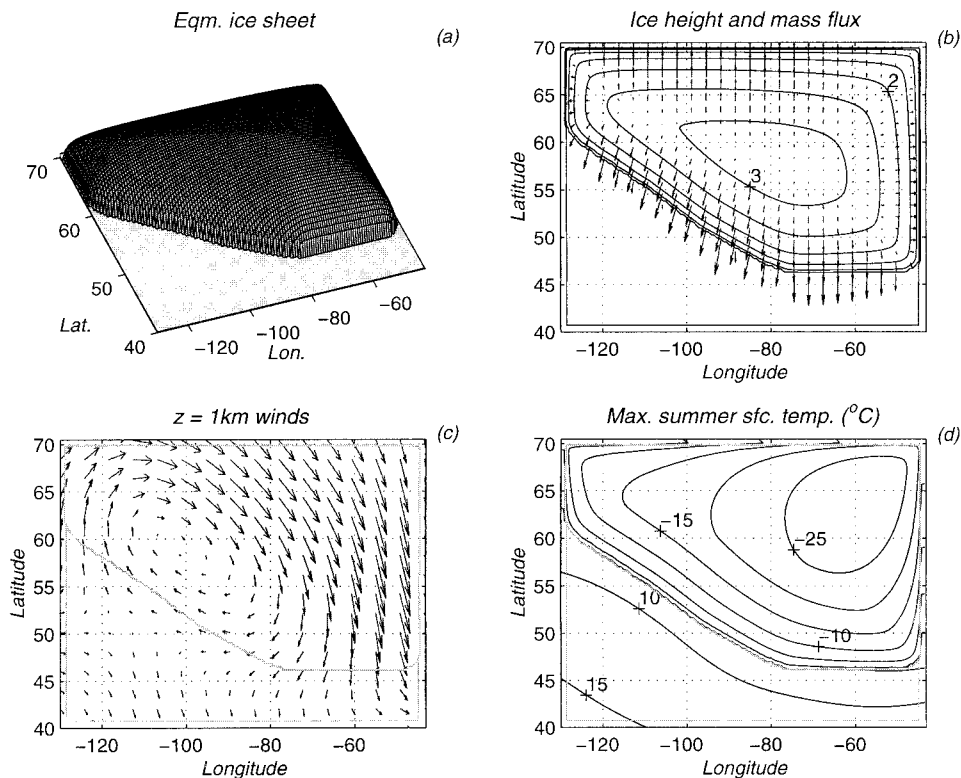


FIG. 7. Model integration with stationary wave feedback included only. The circulation is as calculated by the stationary wave model, but the precipitation is a function only of surface temperature. Same as Fig. 5, except (b) the largest vector plotted corresponds to $1.2 \times 10^5 \text{ m}^2 \text{ yr}^{-1}$. The largest flux of ice (not plotted because of resolution) is $1.7 \times 10^5 \text{ m}^2 \text{ yr}^{-1}$, giving a maximum ice divergence at the margin of 4.4 m yr^{-1} . Plot resolution means flux vectors may deviate slightly from being perpendicular to surface slopes; (c) $z = 1 \text{ km}$ winds as calculated by the stationary wave model. The largest vector plotted corresponds to 15 m s^{-1} ; (d) maximum summer temperature ($^{\circ}\text{C}$).

precipitation rates and also the weaker stationary wave amplitude due to the smaller ice sheet.

While the modeled accumulation rate maximum of 4 m yr^{-1} in Fig. 8c is seen in observations over steep topography in the Pacific Northwest, for example, there are extensive regions over the eastern slopes of the ice sheet where the accumulation is less than 5 cm yr^{-1} . Although they suffer from poor resolution, GCM simulations of the LGM often show a greater accumulation rate than this (e.g., Pollard et al. 2000). It may be that the parameterization used here underestimates the moisture supply by transient weather systems. In that case, the topographic influence would be less pronounced than represented in the model and the situation in reality would be more nearly like that in Fig. 7.

We have so far concentrated on the local response of the ice sheet that forced the stationary wave pattern. However stationary waves are a means for teleconnection across the hemisphere, and Fig. 9 shows the response over the whole of the channel domain for the ice sheet in Fig. 8. Given the channel geometry and the uncertainty about the right basic state, the phase and direction of propagation of the wave patterns remote from the forcing location are liable to be different from

that of a real glacial climate. However, the amplitude of the pattern suggests that the influence of an ice sheet the size of the Laurentide was global in extent and in particular, that the climate over northwestern Europe (and the Fennoscandian ice sheet) would have been strongly influenced by the stationary wave pattern forced upstream by the Laurentide ice sheet. The downstream propagation of the stationary wave patterns gives rise to the possibility of a complicated set of interactions in which each of the two major Northern Hemisphere ice sheet influences evolution of the other.

The remote influence of an ice sheet is mostly downstream, and the presence of atmospheric damping is likely to diminish the relative influence of the Fennoscandian on the Laurentide. The effect of the Tibetan Plateau is uncertain. In the current climate the summertime stationary wave pattern it induces is small, likely because of the poleward shift of the subtropical jet relative to the wintertime (Nigam and Lindzen 1989). However it is possible that the enhanced meridional temperature gradient in a glacial climate would keep the summer subtropical jet anchored close to the Plateau, allowing it to interact with the evolving ice sheets. Figure 9 further implies that the presence of the Laurentide ice sheet

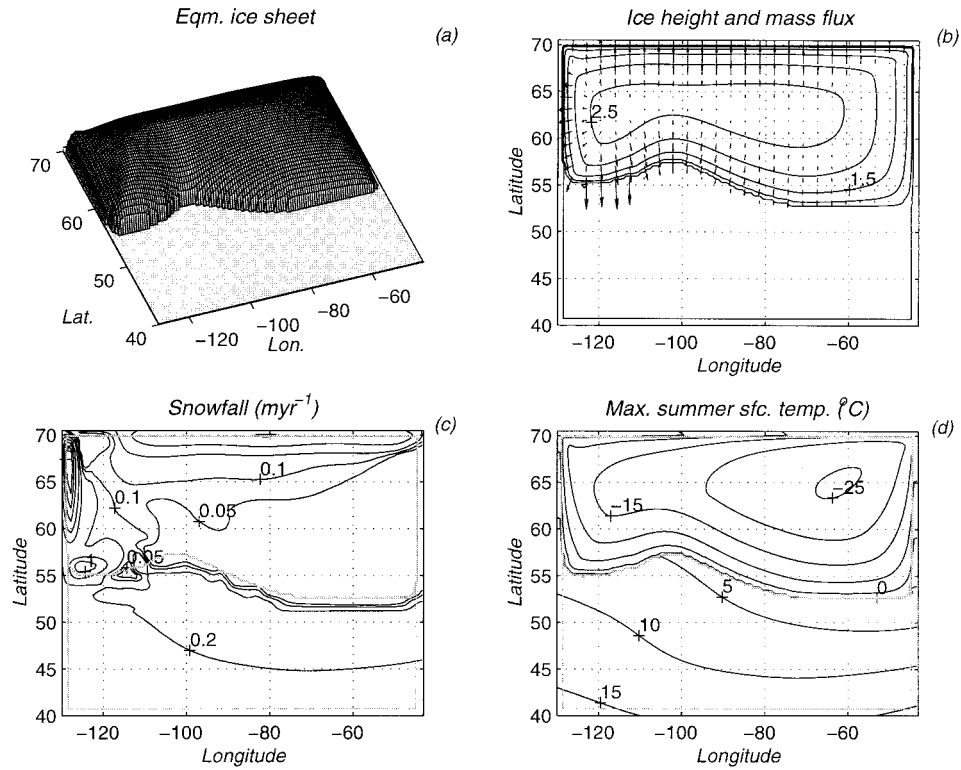


FIG. 8. Model integration with both feedbacks included. The circulation is calculated and the precipitation is enhanced (suppressed) on the windward (leeward) slopes. Same as Fig. 5 except (b) the largest vector plotted corresponds to $0.85 \times 10^5 \text{ m}^2 \text{ yr}^{-1}$. The largest flux of ice (not plotted because of resolution) is $6.0 \times 10^5 \text{ m}^2 \text{ yr}^{-1}$, giving a maximum ice divergence at the margin of 14.9 m yr^{-1} . Plot resolution means flux vectors may deviate slightly from being perpendicular to surface slopes; (c) contour interval used (0.05, 0.1, 0.2, 0.5, 1, 2, 3, 4) m yr^{-1} ; (d) maximum summer temperature ($^{\circ}\text{C}$).

would strongly affect the wind stress over the North Atlantic basin, altering the wind-driven ocean circulation.

e. Stationary wave sensitivities

We have so far only considered integrations for one sensitivity of stationary wave response, while GCM simulations have displayed a range of responses to the same imposed boundary conditions (e.g., Manabe and Broccoli 1985; Kutzbach and Guetter 1986; Hall et al. 1996). We therefore show integrations of what might be called a “weak” and a “strong” stationary wave sensitivity. This is done by using the different basic states shown in Fig. 2. In these integrations, the qualitative shape of the equilibrium ice sheets remains the same (Fig. 10), which means that the physics controlling the interaction is the same and robust to a variety of amplitudes. The weak sensitivity generates an east–west temperature gradient of about $\sim 4^{\circ}\text{C}$ and the strong sensitivity gives $\sim 13^{\circ}\text{C}$. There are several other parameters that affect the amplitude and phase of the response, such as \bar{U}_f and τ (Roe 1999), but GCM simulations of the atmospheric response to LGM ice sheets seem to lie within the amplitude range that Fig. 10 reflects.

The eastern sector of the ice sheet follows the summer temperature patterns. The strong basic state produces an eastward phase shift of about 15 degrees in the atmospheric response compared to Fig. 8. The minimum temperatures therefore occur slightly off the east coast of the continent. This means that despite a larger amplitude in the temperature pattern, the ice sheet evolving with the strong stationary wave sensitivity is only about as extended as in Fig. 8. There are also competing processes on the western sector. For example, for the strong stationary wave sensitivity, the eastward phase shift produces more southwesterly winds in the west, increasing precipitation there that offsets the extra melting due to the warmer temperatures. The behavior of this lobe of the ice sheet illustrates how the different aspects of the atmospheric response play off against each other to create the final ice sheet configuration.

f. Multiple equilibria

For fixed accumulation and ablation fields an ice sheet evolves such as to redistribute ice between the accumulation and ablation regions. Studies using one-dimensional ice sheet models and simplified mass balance parameterizations have often shown that two equilib-

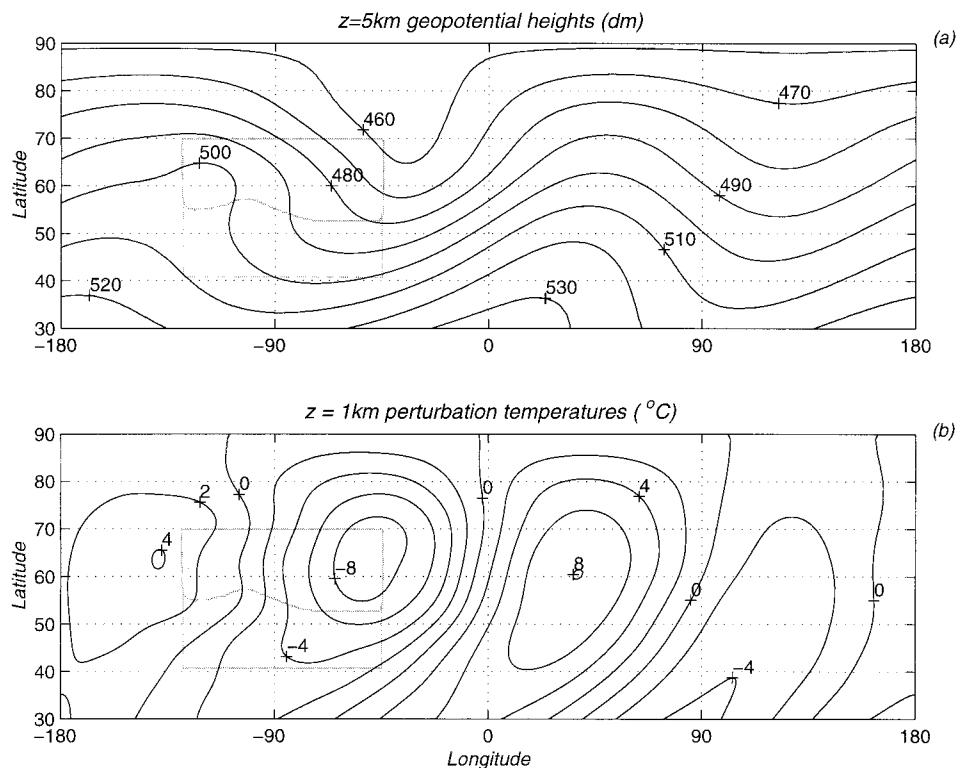


FIG. 9. Global patterns of the stationary wave fields generated by the ice sheet in Fig. 8. (a) Here $z = 5$ -km geopotential heights (dm), and (b) temperature perturbation from zonal mean at $z = 1$ km ($^{\circ}\text{C}$). The forcing ice sheet is faintly outlined. The stationary wave pattern exerts a significant influence on climate downstream of the forcing region.

rium solutions can exist, although only one is generally stable (e.g., Weertman 1976). Ice age modeling efforts using EBMs do not usually consider this possibility. Moreover, if the ice sheet itself is changing the climate patterns, then there is no guarantee of a single equilibrium solution and the final ice sheet may depend on the way it changed the climate forcing during its evolution.

The model integrations presented so far in the paper have all been made from initially ice-free conditions. Figure 11 shows the steady equilibrium ice sheets that result from integrations that are identical except for the use of widely different initial ice sheet shapes. Although the basic shape of the resulting equilibrium ice sheets is the same, in each case there are some differences in volume, area, and height (up to a 30% difference in equilibrium volume). The differences are a consequence of the way in which the initial ice sheet caused different initial distributions of accumulation and ablation that in turn sustained different ice sheet evolutions.

4. Ice sheet growth

The one dimensional model of Roe and Lindzen (2001) suggested that the time dependence of an ice sheet would be influenced by the stationary wave feedback. For example, if a growing ice sheet is inducing colder temper-

atures at its margin (due to circulation changes), then the growth rate might be expected to be larger.

Since cold temperatures extend over most of the ice sheet because of the location of the high pressure, we should expect a greater overall growth rate. Figure 12 shows the time evolution of the ice sheets shown in Figs. 5–8, starting from no ice. The ice area starts at a finite value because the climate is held constant rather than being gradually cooled. For integrations including topographic precipitation effects, the initial peak at around 4 kyr in the maximum height represents the large local accumulation that builds up before the ice dynamics has a chance to get going and redistribute the ice mass. In both volume and area, the largest growth rate is for the integration including only the stationary wave feedback. The mechanism is the same as Roe and Lindzen (2001): cold temperatures induced by the circulation changes allows the ice to accumulate over a larger area. However when both feedbacks are included there is a competing process: the generally downslope northerly winds reduces the accumulation rate over most of the ice sheet, and therefore it is unable to grow as fast. That the two processes almost exactly cancel and restore the growth rate to that of the no-feedback integration is largely a coincidence. Though the mechanisms will always tend to counteract each other, a different set of

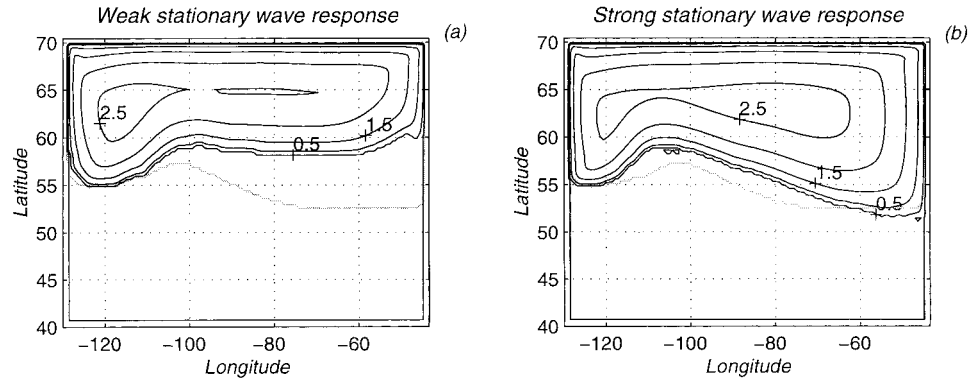


FIG. 10. Equilibrium ice sheets for different stationary wave sensitivities. (a) The weak stationary wave response, (b) strong stationary wave response. The ice sheet from Fig. 8 is outlined faintly in both (a) and (b). The details of the integrations are described in the text.

parameters would change the relative balance between the feedbacks and affect the growth rate accordingly. The results in Fig. 12 highlight the importance of accounting for changing accumulation and ablation patterns during an ice sheet's evolution.

A more realistic situation for an evolving ice sheet is one where it initiates on high ground and gradually

evolves in a cooling climate. Accordingly an integration was performed in which a 1-km high Gaussian-shaped plateau was placed in the central northern part of the continent. Initially the model climate is such that year-round accumulation occurred only on this plateau. A cooling of 8.5°C is imposed on the whole domain over the first 15 kyr of the integration, after which the climate

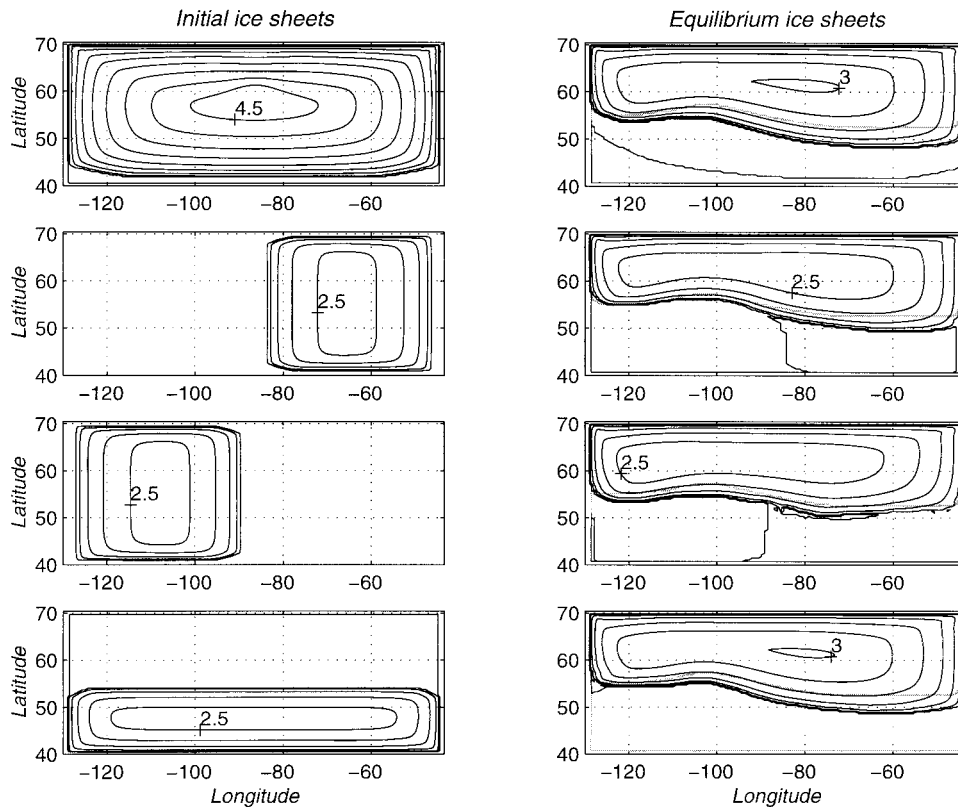


FIG. 11. Integrations for widely different initial ice sheet conditions. The left-hand panels show the initial ice sheets used and the right-hand panels show the corresponding equilibrium ice sheets. The ice sheet from Fig. 8 is outlined faintly on the right-hand panels. The equilibrium ice sheets differ in area and height. The grid-scale details are likely numerical artifacts. Contours are every 0.5 km. The faint signature of the bedrock depression from the initial ice sheets can be seen in the right-hand panels.

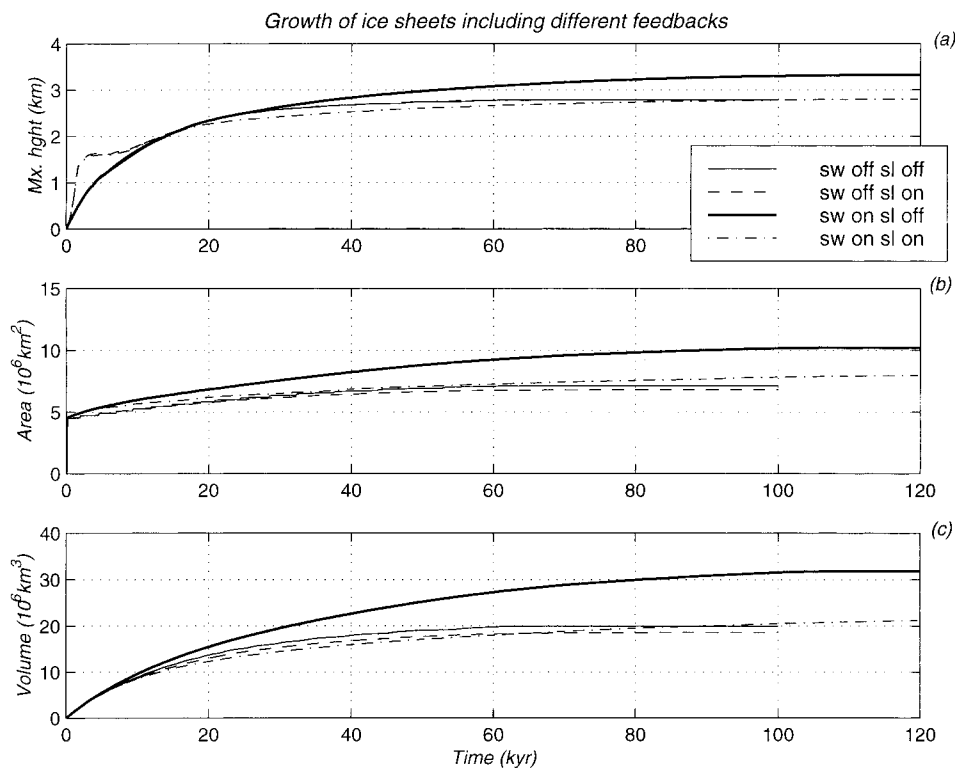


FIG. 12. Growth to equilibrium for ice sheet integrations with different combinations of feedbacks included. Here SW refers to the stationary wave feedback, SL (for slope) refers to the topographic precipitation feedback. (a) The maximum ice sheet height (km), (b) ice sheet area (10^6 km^2), (c) ice sheet volume (10^6 km^3).

is the same as used in the previous section. Figure 13 shows the very strong influence of topographic precipitation on the early evolution of the ice sheet. Large accumulation rates occur on the windward slopes, and raises the surface height so it becomes cold enough for the ice to remain. The steep surface slopes cause a large westward flux of ice that is tracked by the precipitation maxima. In this way, a rapid westward spreading of the ice takes place. The spreading is dependent on the precipitation rate on the western slopes and therefore on the parameter b [Eq. (6)]. If the precipitation rate is artificially capped at 1 m yr^{-1} , the ice sheet takes several thousand more years to reach the west coast.

The evolving precipitation pattern has most significance for the growth of the Laurentide ice sheet which initiated away from the coast over Keewatin and Quebec, Canada (Clark et al. 1993). It is relatively less important for the Fennoscandian ice sheet that initiated on the high ground of Scandinavia, closer to the coast.

It is only after about 6 kyr of growth that the climate has cooled down sufficiently to allow year-round accumulation east of the plateau. By this time the ice sheet has almost reached the west coast, and a large mass of ice has accumulated that is substantial enough to generate a small stationary wave. This influences the evolution of the ice sheet in the east, as can be seen by the

nonzonal evolution of the ice there. Larger changes in the ice sheet would be reflected across the Northern Hemisphere via patterns like those in Fig. 9, potentially affecting the evolution of other ice sheets.

After 15 kyr, the climate cooling is completed and the remaining changes in the ice sheet are the consequence of the redistribution of the ice mass through flow, and the growth of the stationary wave that the topography generates.

5. Summary and discussion

The results of this study show that continental-scale ice sheets cause changes to the stationary pattern that are a zeroth-order forcing in glacial climates: local climate changes due to the induced circulation are as large as glacial to interglacial differences and can exert a powerful influence on the evolution of an ice sheet.

The atmospheric response to ice sheet topography is a high pressure anticyclonic circulation centered over the western flank of the ice sheet producing cold northerly winds over most of the ice sheet. In equilibrium, the land-based southern margin of an ice sheet is largely determined by the pattern of summer temperatures. The exception to this is where the topographically induced precipitation generates high accumulation on the wind-

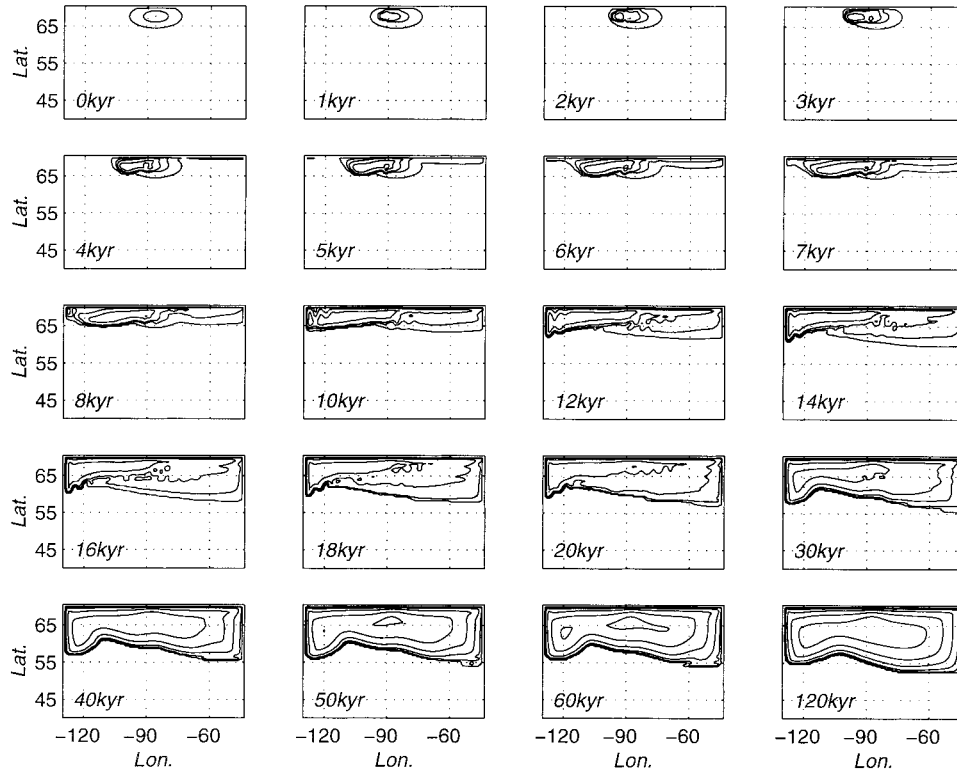


FIG. 13. Contour time series (not evenly spaced in time) for growth to equilibrium for ice sheet initiating on a plateau. Climate is cooled by 8.5°C over the first 15 kyr. Final climate is same as Fig. 8. Height contours every 0.5 km. Early growth is dominated by the topographic precipitation, subsequent growth by ice flow, and adjustment to the induced stationary wave pattern.

ward slopes. In this case, the local accumulation becomes a significant part of the ice mass budget and contributes to the shape of the ice sheet. The physics of the interaction is robust for a wide range of model sensitivities, but the quantitative details are affected by the choice of model parameters, and therefore on the relative strength of the feedbacks in nature. The pattern of temperatures forced by the topography (warm in the west and cool to the east) may help to explain the absence of ice over Alaska at the LGM, and the extension of the Laurentide ice sheet deep into New England (Roe 1999; Vettoretti et al. 2000).

An ice sheet of the size of those at the LGM has a big influence on remote climates via the stationary wave it creates. In particular the results suggest that the Laurentide ice sheet may have contributed a significant warming to the climate over Europe, and therefore influenced the evolution of the Fennoscandian ice sheet. The phase and amplitude of the warming is uncertain, not least because of the uncertainties in the appropriate basic state to use for a glacial climate. GCM simulations can only provide guidelines. For example the LGM climates produced by the current suite of GCM simulations, assessed as part of the Paleoclimate Model Intercomparison Project, are not consistent with the

known configuration of the ice sheets (Pollard et al. 2000).

If an ice sheet initiates away from a western coastline, its early growth is dominated by the enhanced topographic precipitation on the windward side, causing rapid westward propagation of the ice margin toward the coast. It is likely this occurred during the evolution of the Laurentide ice sheet. Subsequent development of the ice sheet is controlled by large-scale climate cooling and the circulation changes caused by the stationary wave response to the building ice sheet.

The model presented in this paper was simplified in several important ways, and the possible consequences need to be discussed. We neglected an ice sheet's thermal influence on the atmosphere, whereas observations show there is a steady cooling of the air overlying an ice sheet (e.g., Ohmura et al. 1994). Imposing a plausible cooling of 20 Wm^{-2} over the model ice surface produces an anticyclonic circulation over the ice sheet, but with a smaller amplitude than the topographic response (Roe 1999). This is consistent with the winter results of Cook and Held (1988) in which most of the atmospheric response was explained by the linear topographic forcing. However summer is the important season for creating the patterns of melting, and the mod-

el's linear damping on temperature is not a very physical treatment of the exchange of sensible and latent heat above an ice surface. Further, we have omitted the feedback between stationary waves and storm tracks: the stationary waves control the location of storm tracks, and the latent heat released within the storm tracks acts to drive in part the stationary wave pattern (e.g., Hoskins and Karoly 1981). Kageyama et al. (1999) show that GCMs tend to produce an eastward shift of the storm tracks at the LGM, relative to the present. If thermal forcing is indeed important to changes in a glacial climate then we emphasize that the feedbacks created by the induced circulations would still act in the way discussed here, with the summer melting and the topographic precipitation patterns creating the ice sheet configuration.

Another potentially important issue is the moisture supply to the interior of the ice sheet. The parameterization used here makes no distinction between locations close to moisture sources, such as the west coast, and locations in the continental interior. Nor does it conserve water mass along an air parcel trajectory. It is possible that the accumulation might be limited by the rate at which moisture can be supplied. For example the growth of ice sheets might be inhibited in the lee of preexisting mountain ranges. A moisture scheme such as that of Sanberg and Oerlemans (1983) that crudely accounts for moisture transport might be able to be used to study this question.

Finally, we have shown that because the ice sheet influences the climate fields that force it, multiple equilibrium solutions exist. We speculate a much richer set of interactions is a possibility if some of the model simplifications are removed. With realistic geography and topography, and depending on local climate conditions, an ice sheet may initiate in one location or another, or in several places simultaneously. The different ways that the climate forcing is affected may create entirely different evolution histories for the ice sheet. The stationary wave patterns from other sources (e.g., sensible and latent heating) also likely changes during a glacial cycle and further influences the evolution (Yin and Battisti 2001). Thus the configuration of an ice sheet at a glacial maximum (say) may be a function of the whole climate history up to that point in the glacial cycle. Conceivably also, that history might be partially deduced from the shape of the ice sheet. For instance it might be that Alaska and Siberia remain deglaciated only for certain climate trajectories. Clearly an important next step is to reconcile the mechanisms demonstrated here to the geological record.

Acknowledgments. This work was partly supported by Grant ATM9813795 from the National Science Foundation, Grant DEFG02-93ER61673 from the Department of Energy, and Grant NAG5-5147 from NASA. Valuable conversations with K. Emanuel, D. Battisti, and D. MacAyeal are much appreciated. Thanks to Ralf

Greve and Veronique Bugnion for much assistance with the SICOPOLIS model, and we are also grateful to Charlie Raymond and two anonymous reviewers for their insightful comments on the manuscript.

APPENDIX

Integration of Precipitation Formulation

In this appendix we show the calculation of the precipitation rate using a distribution of vertical velocities described in section 2d. The precipitation rate for fixed T_s is the integral of Eq. (6) over the fraction of time for which the vertical velocity is large enough to give precipitation:

$$P = e_{\text{sat}}(T_s) \int_{-a/b}^{\infty} (a + bw')f(w') dw' \quad (\text{A1})$$

with

$$f(w')dw' = \frac{e^{-\alpha^2(w'-w)^2}dw'}{N}. \quad (\text{A2})$$

From the normalization requirement that $\int_{-\infty}^{\infty} f(w') dw' = 1$, we get, using standard integrals, that $N = \sqrt{\pi}/\alpha$.

If we substitute a dummy variable $x = w' - w$, then Eqs. (A1) and (A2) become

$$P = \frac{\gamma_1 e_{\text{sat}}}{N} \int_{-x_0}^{\infty} (x_0 + x)e^{-\alpha^2 x^2} dx, \quad (\text{A3})$$

where $x_0 = a/b + w$. Equation (A3) can be rewritten as

$$P = \frac{be_{\text{sat}}}{N} \left(x_0 \int_0^{\infty} e^{-\alpha^2 x^2} dx + \frac{x_0^2}{|x_0|} \int_0^{|x_0|} e^{-\alpha^2 x^2} dx + \int_{-x_0}^{\infty} xe^{-\alpha^2 x^2} dx \right). \quad (\text{A4})$$

The modulus of $|x_0|$ in the second term on the rhs of Eq. (A4) accounts for the possibility that x_0 might be negative. The above integrals have standard analytic solutions, which means Eq. (A4) can be written as

$$P = \frac{be_{\text{sat}}}{N} \left[x_0 \frac{\sqrt{\pi}}{2\alpha} + \frac{x_0^2}{|x_0|} \frac{\sqrt{\pi}}{2\alpha} \text{erf}(\alpha|x_0|) - \frac{1}{2\alpha^2} |e^{-\alpha^2 x^2}|_{-x_0}^{\infty} \right]. \quad (\text{A5})$$

Here $\text{erf}(\alpha x_0)$ is the error function. Abramowitz and Stegun (1965) give the following very accurate asymptotic series expansion for the error function:

$$\text{erf}(y) = 1 - (\gamma_1 t + \gamma_2 t^2 + \gamma_3 t^3)e^{-y^2}, \quad (\text{A6})$$

where $t = 1/(1 + \gamma_0 y)$, and $\gamma_0, \gamma_1, \gamma_2$, and γ_3 are all constants. Equation (A5) can therefore be directly calculated to give the precipitation rate for a given T_s .

REFERENCES

- Abramowitz, M., and I. A. Stegun, 1965: *Handbook of Mathematical Functions with Formulas, Graphs, and Mathematical Tables*. Dover Publications, 1046 pp.
- Braithwaite, R. J., and O. B. Oleson, 1989: Calculation of glacier ablation from air temperature, West Greenland. *Glacier Fluctuation and Climate Change*, J. Oerlemans, Ed., Kluwer Academic, 219–233.
- Calov, R., and K. Hutter, 1996: The thermomechanical response of the Greenland ice sheet to various climate scenarios. *Climate Dyn.*, **12**, 243–260.
- Clark, P. U., and Coauthors, 1993: Initiation and development of the Laurentide and Cordilleran ice sheets following the last interglaciation. *Quat. Sci. Rev.*, **12**, 79–114.
- Cook, K. H., and I. M. Held, 1988: Stationary waves of the ice age climate. *J. Climate*, **1**, 87–89.
- Crowley, T. J., and G. R. North, 1991: *Paleoclimatology*. Oxford University Press, 339 pp.
- Greve, R., 1997: Application of a polythermal three-dimensional ice sheet model to the Greenland ice sheet: Response to steady state and transient climate scenarios. *J. Climate*, **10**, 901–918.
- Hall, N. M. J., P. J. Valdes, and B. Dong, 1996: The maintenance of the last great ice sheets: A UGAMP GCM study. *J. Climate*, **9**, 1004–1019.
- Holton, J. R., 1992: *An Introduction to Dynamic Meteorology*. Academic Press, 511 pp.
- Hoskins, B. J., and D. J. Karoly, 1981: The steady linear response of a spherical atmosphere to thermal and orographic forcing. *J. Atmos. Sci.*, **38**, 1179–1196.
- Hutter, K., 1983: *Theoretical Glaciology: Material Science of Ice and the Mechanics of Glaciers and Ice Sheets*. D. Reidel, 510 pp.
- Kageyama, M., P. J. Valdes, G. Ramstein, C. Hewitt, and U. Wypulla, 1999: Northern Hemisphere storm tracks in present day and last glacial maximum climate simulations: A comparison of the European PMIP models. *J. Climate*, **12**, 742–760.
- Kalnay, E., and Coauthors, 1996: The NCEP/NCAR 40-Year Reanalysis Project. *Bull. Amer. Meteor. Soc.*, **77**, 437–471.
- Kutzbach, J. E., and P. J. Guetter, 1986: The influence of changing orbital parameters and surface boundary conditions on climate simulations for the past 18 000 years. *J. Atmos. Sci.*, **43**, 1726–1759.
- Lindzen, R. S., 1994: The effect of concentrated PV gradients on stationary waves. *J. Atmos. Sci.*, **51**, 3455–3466.
- , and G. H. Roe, 1997: The effect of concentrated PV gradients on stationary waves: Correction. *J. Atmos. Sci.*, **54**, 1815–1818.
- Manabe, S., and A. J., Broccoli, 1985: The influence of continental ice sheets of an ice age. *J. Geophys. Res.*, **90**, 2167–2190.
- Milankovitch, M., 1941: Canon of insolation and the ice age problem (in Yugoslavian). K. Serb. Acad. Beorg. Special Publication 132. (English translation by Israel Program for Scientific Translations, Jerusalem, 1969, published by the U.S. Department of Commerce and the National Science Foundation.)
- Nigam, S., and R. S. Lindzen, 1989: The sensitivity of stationary waves to variations in the basic state zonal flow. *J. Atmos. Sci.*, **46**, 1746–1768.
- Ohmura, A., T. Konzelmann, M. Rotach, J. Forrer, M. Wild, A. Abe-Ouchi, and H. Toritani, 1994: Energy balance for the Greenland ice sheet by observation and model computation. *Snow and Ice Covers: Interaction with the Atmosphere and Ecosystems*, H. G. Jones et al., Eds., IAHS Publ. 223, IAHS Press, 85–94.
- Paterson, W. S. B., 1994: *The Physics of Glaciers*. 3d ed. Pergamon Press, 480 pp.
- Pedlosky, J., 1992: *Geophysical Fluid Dynamics*. Springer-Verlag, 710 pp.
- Peixoto, J. P., and A. H. Oort, 1992: *Physics of Climate*. American Institute of Physics, 520 pp.
- Pollard, D., 1982: A simple model yields realistic 100 kyr glacial cycles. *Nature*, **296**, 334–338.
- , and PMIP Participating Groups, 2000: Comparisons of ice sheet surface mass budgets from Paleoclimate Modeling Intercomparison Project (PMIP) simulations. *Global Planet. Change*, **24**, 79–106.
- Reeh, N., 1991: Parameterization of melt rate and surface temperature on the Greenland ice sheet. *Polarforschung*, **59**, 113–128.
- Roe, G. H., 1999: Wobbly winds in an ice age: The mutual interaction between the great continental ice sheets and atmospheric stationary waves. Ph.D. thesis, Massachusetts Institute of Technology, 236 pp. [Available from Massachusetts Institute of Technology, 77 Massachusetts Ave., Cambridge, MA 02139-4307.]
- , and M. R. Allen, 1999: A comparison of competing explanations for the 100,000-yr ice age cycle. *Geophys. Res. Lett.*, **26**, 2259–2262.
- , and R. S. Lindzen, 2001: A one-dimensional model for the interaction between continental-scale ice sheets and atmospheric stationary waves. *Climate Dyn.*, in press.
- Sanberg, J. A. M., and J. Oerlemans, 1983: Modeling of Pleistocene European ice sheets: The effect of upslope precipitation. *Geol. Mijnbouw*, **62**, 267–273.
- Smith, R. B., 1979: The influence of mountains on the atmosphere. *Advances in Geophysics*, Vol. 21, Academic Press, 87–230.
- Tangborn, W. V., and M. Simont, 1988: *Glaciers*. 2d ed. Harper and Row, 32 pp.
- Tarasov, L., and W. R. Peltier, 1997: Terminating the 100kyr ice age cycle. *J. Geophys. Res.*, **102**, 21 655–21 693.
- Vettoretti, G., W. R. Peltier, and N. A. McFarlane, 2000: Global water balance and atmospheric water vapor transport at the last glacial maximum: climate simulations with the CCCma atmospheric general circulation model. *Can. J. Earth Sci.*, **37**, 769–793.
- Weertman, J., 1976: Milankovitch solar radiation variations and ice age ice sheet sizes. *Science*, **261**, 17–20.
- Yin, J. H., and D. S. Battisti, 2001: The importance of tropical sea surface temperature patterns in simulations of Last Glacial Maximum climate. *J. Climate*, **14**, 565–581.